# High Dopant Activation And Low Damage P+ USJ Formation

John Borland[1], Seiichi Shishiguchi[2], Akira Mineji[2], Wade Krull[3], Dale Jacobson[3], Masayasu Tanjyo[4], Wilfried Lerch[5], Silke Paul[5], Jeff Gelpey[5], Steve McCoy[5], Julien Venturini[6], Michael Current[7], Vladimir Faifer[7], Robert Hillard[8], Mark Benjamin[8], Tom Walker[9], Andrzej Buczkowski[9], Zhiqiang Li[9] and James Chen[10]

[1]J.O.B Technologies, Aiea, HI; [2]NEC Electronics Corp., Sagamihara, Japan; [3]SemEquip, North Billerica, MA; [4]Nissin Ion Equipment, Kyoto, Japan; [5]Mattson Technology, Fremont, CA; [6]Sopra Optical Solutions, Bois-Colombes, France; [7]Frontier Semiconductor, San Jose, CA; [8]Solid State Measurements, Pittsburgh, PA; [9]Accent Optical Technologies, Bend, OR; and [10]Four Dimensions, Hayward, CA

**Abstract.** High dopant activation and low damage p+ ultra-shallow junctions (USJ) 15-20nm deep for 45nm node applications have been realized using $B_{10}H_{14}$ & $B_{18}H_{22}$ implant species along with flash, laser or SPE diffusion-less activation annealing techniques. New USJ metrology techniques were employed to determine: 1) dopant activation level and 2) junction quality (residual implant damage) using both contact and non-contact methods.

**Keywords:** ultra-shallow junction, boron, decaborane, octa-decaborane, flash annealing, laser annealing, SPE annealing, USJ metrology
**PACS:** 85..40.Ry

## INTRODUCTION

For the 45nm node, the p+ USJ for extension varies between 15nm to 20nm deep depending on the device application and trade-offs between dopant activation, junction depth (Xj) and junction quality for high performance (HP), low operating power (LOP) and low-standby power (LSTP) logic devices. To minimize boron dopant diffusion, high temperature >1300°C (flash or laser) or low temperature 650°C SPE annealing are available resulting in <5nm of dopant movement. To eliminate dopant channeling pre-amorphization implantation (PAI) is usually used. PAI and/or co-implantation can lead to higher dopant activation, however, the residual end-of-range (EOR) damage can also result in high damage junctions when using these advanced dopant activation techniques with minimal dopant diffusion [1,2]. For this reason we investigated alternative p+ dopant species to B and $BF_2$ such as $B_{10}H_{14}$ and $B_{18}H_{22}$ because of their self-amorphization effects avoiding PAI and EOR damage to achieve low damage high quality junctions [3].

## EXPERIMENTATION

Boron 500eV/1E15/cm² dose equivalent implants were performed on one hundred, 200mm n-type wafers using B, $BF_2$, $B_{10}H_{14}$ and $B_{18}H_{22}$ implant species. The implants were performed into crystalline silicon or 11.5nm deep amorphous silicon layer using Ge 5keV/5E14/cm² for PAI. Both batch and serial implanters were used for implant signature comparison.

Dopant activation was achieved using: 1) spike annealing at 1080°C or 1000°C at Mattson/Germany, 2) msec flash annealing at 1300°C at Mattson/Canada, 3) 200nsec sub-melt laser annealing at Sopra/France or 4) 5sec 650°C SPE annealing at Mattson/Germany. Sheet resistance (Rs) was measured with non-contact junction photo-voltage (JPV) at Frontier and contact non-penetrating 4 point probe (4PP) using elastic material (EM) probes at Solid State Measurements (SSM) and mercury (Hg) probes at Four Dimensions (4D). The electrically active surface dopant level/density was measured by a C-V technique (Nsurf) at SSM. SIMS analysis at NEC was used to determine the boron chemical density depth profile and X-TEM to evaluate the amorphous layer depth and after anneal residual implant EOR damage. After anneal junction quality was determined by junction leakage measurement using JPV at Frontier. Silicon crystal lattice damage levels were measured by photo-luminescence imaging (PLi) at Accent on as-implanted and after annealed wafers.

## RESULTS & DISCUSSION

Figures 1 and 2 shows SIMS boron depth profiles for B and $B_{18}H_{22}$ after each anneal. Without Ge-PAI, evidence of channeling for B starts at 8E18/cm³ as shown in Fig. 1a and for $B_{18}H_{22}$ it starts at 4E18/cm³ as shown in Fig. 2a. Table 1 shows the SIMS determined chemical junction depth (Xj) defined at 1E18/cm³ for all the conditions studied. Channeling for B and $BF_2$ is about 9nm, for $B_{10}H_{14}$ is about 4nm and for $B_{18}H_{22}$ is

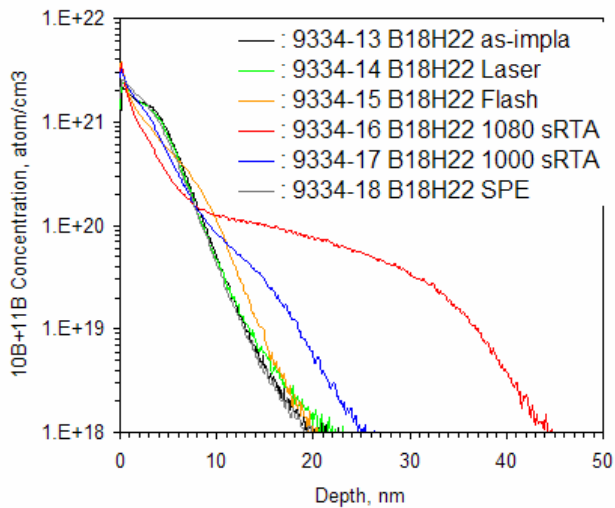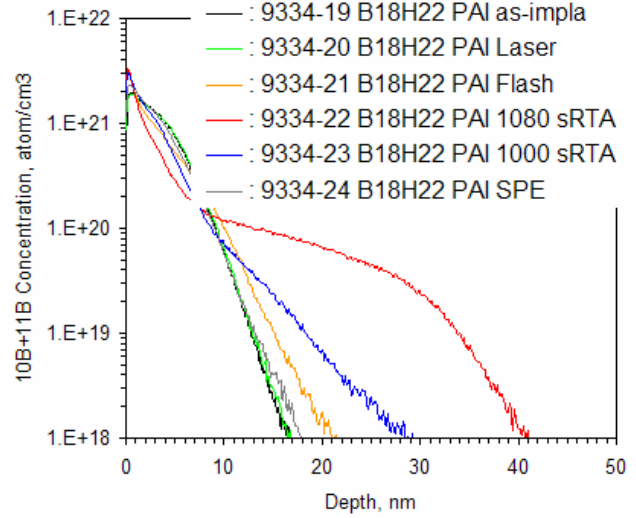about 3nm. PAI results in greater boron dopant diffusion with lamp based annealing.
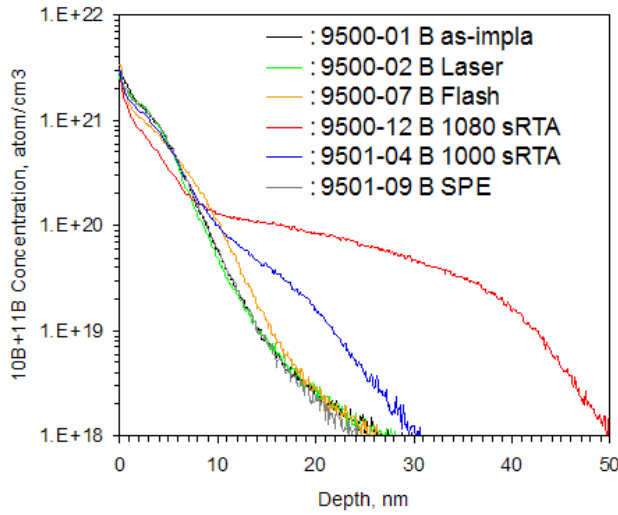


a)
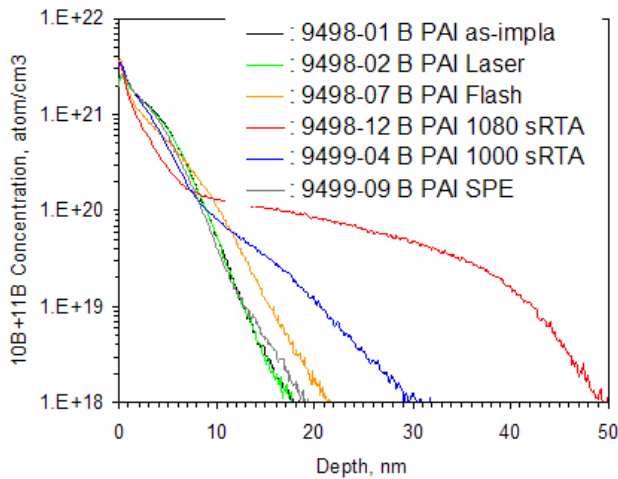


b)

**Figure 1.** a) B and b) PAI+B SIMS results.



a)



b)



b)

**Figure 2.** $B_{18}H_{22}$ & PAI+$B_{18}H_{22}$ SIMS results.

**TABLE 1.** SIMS determined Xj depth in nm at $1E18/cm^3$ and dopant movement.

| Dopant | Control | Spike/1080 | Spike/1000 | Flash | Laser | SPE/650 |
|---|---|---|---|---|---|---|
| B11 | 26.9 | 50.1+23.2 | 30.4+3.5 | 25.9-1.0 | 26.8-.1 | 24.1-2.8 |
| +PAI | 17.9 | 49.3+31.4 | 30.4+12.5 | 21.5+3.6 | 18.0+.1 | 19.4+1.5 |
| | | | | | | |
| BF2 | 25.1 | 40.6+15.5 | 27.6+2.5 | 25.2+.1 | 24.0-1.1 | 22.0-3.1 |
| +PAI | 16.6 | 39.6+23.0 | 26.9+10.3 | 21.0+4.4 | 17.0+.4 | 17.7+1.1 |
| | | | | | | |
| B10-serial | 18.7 | 36.5+17.8 | 23.2+4.5 | 17.5-1.2 | 19.8+1.1 | 17.4-1.3 |
| +PAI | 14.8 | 36.5+21.7 | 29.3+14.5 | 19.8+5.0 | 15.2+.4 | 16.8+2.0 |
| | | | | | | |
| B10 | 20.0 | 36.6+16.6 | 22.5+2.5 | 18.6-1.4 | 19.2-.8 | 18.0-2.0 |
| +PAI | 15.5 | 36.6+21.1 | 28.5+13.0 | 20.9+5.4 | 15.9+.4 | 16.9+1.4 |
| | | | | | | |
| B18 | 19.7 | 44.7+25.0 | 25.4+5.7 | 20.0+.3 | 21.0+1.3 | 19.4-.3 |
| +PAI | 16.6 | 41.1+24.5 | 28.8+12.2 | 21.6+5.0 | 16.8+.2 | 18.2+1.6 |

The 1080°C spike anneal resulted in 15.5-31.4nm of dopant diffusion. When the temperature was reduced to 1000°C only 2.5-14.5nm of diffusion occurred. With flash annealing -1.4 to +5.4nm of diffusion was observed. With laser annealing -1.1 to +1.3nm of dopant movement and with SPE -3.1 to +2nm of dopant movement.

PLi analysis was used to get a full wafer image mapping of the as-implanted damage and after annealing damage recovery (residual implant damage). The as-implanted PAI wafers all had high PLi values between 72-75 due to the 11.5nm deep Ge amorphous layer while the non-PAI wafers had PLi values between 41-46. For the wafers receiving the 1080°C spike anneals and flash anneals complete damage recovery was detected as shown in Fig. 3a&b with PLi values below 14 but the $BF_2$ samples always had the highest PLi values suggesting a F effect that dominates even over Ge-PAI. The PLi results for 650°C SPE annealing is shown in Fig. 4. The EOR damage from PAI and $BF_2$ implants resulted in PLi

values between 25-29 while B residual implant damage values were 31. The molecular dopant species without PAI had the lowest PLi values between 14-18 suggesting complete damage recovery of the self-amorphizing layer.
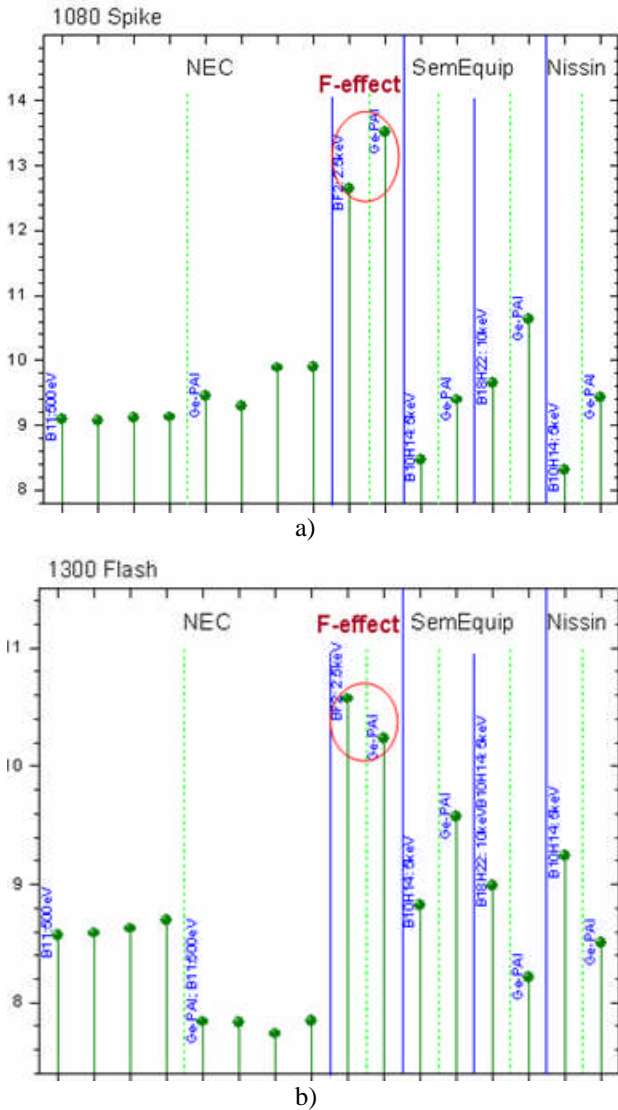




**Figure 3**. a) 1080°C spike PLi results and b) Flash PLi results.
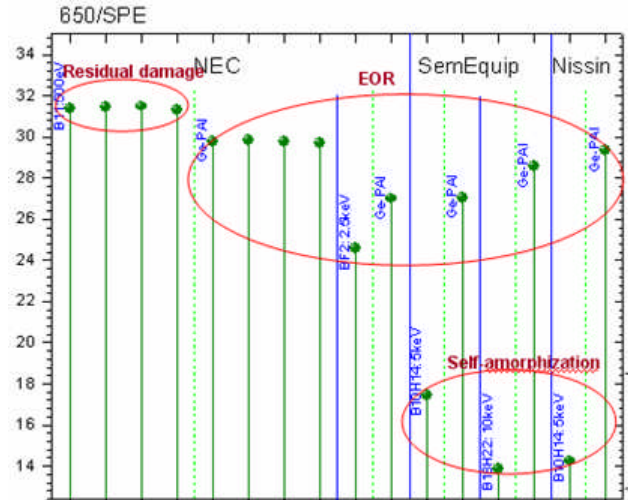


**Figure 4.** 650°C SPE PLi results.

Figures 5-7 shows X-TEM results for the Flash, SPE and laser annealing respectively. With the high temperature flash anneal all the samples were clean with no evidence of residual implant damage nor EOR damage from the amorphous layer. The PLi values were 8 to 9 in Fig. 5 with JPV leakage all <1E-7A/cm2. With the SPE anneal as shown in Fig. 6 residual implant damage within the top 6nm of the surface could be observed for the B implant as reflected by the PLi value of 30 and leakage of 1E-5A/cm2. The $BF_2$ sample showed well defined EOR damage resulting in a PLi value of 25 and leakage of 1E-6A/cm2. $B_{18}H_{22}$ was clean with a PLI value of 14 and leakage of 2E-7A/cm2 while with Ge-PAI well defined EOR damage could be seen with a PLi value of 29 and leakage of 2E-5A/cm2. After laser annealing random residual damage could also be seen for the B sample with a PLi of 19 and leakage of 3E-7A/cm2 while the $BF_2$ sample shows EOR damage as well as a 3nm surface amorphous layer with PLi of 27 and leakage of 3E-6A/cm2. The B18H22 sample was again clean with a PLi of 13 and leakage of 1E-7A/cm2 while with Ge-PAI an 11.5nm of amorphous layer remained suggesting no recrystalization and the PLi value was high around 55 and leakage of 2E-2A/cm2. In fact all the Ge-PAI samples remained amorphous after laser annealing with PLi values between 55-65 and remained n-type, no electrical activation/conversion to p-type.
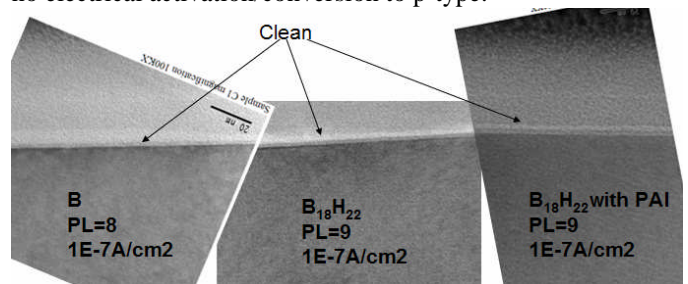


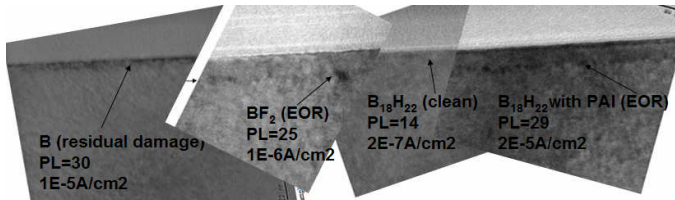**Figure 5.** X-TEM of flash annealed samples.

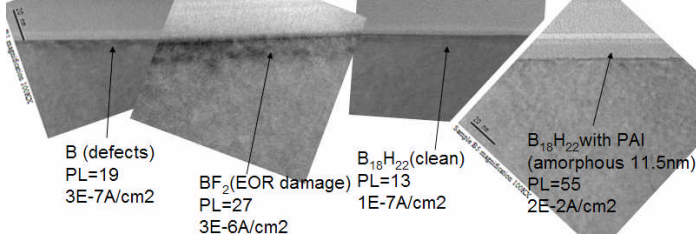**Figure 6.** X-TEM of $650^{\circ}$C SPE annealed samples.



**Figure 7.** X-TEM of laser annealed samples.

The unique signature of each annealing technique can be seen by full wafer PL imaging as shown in Fig. 8. The gradient are magnified in these figures; the actual variations are quite small. Spike annealing shows a center to edge gradient with the highest PLi of 10.3, in the center and 9.2 at the edge; flash annealing shows dark spots (8.1PLi) where the wafer lifters are located (an artifact of the earlier version of the tool used to process the wafers) compared to the other bright areas (7.7PLi); the SPE signature is slightly darker towards the center (35.9PLi) compared to the edge (32.4PLi); and laser annealing shows a step and repeat checkerboard pattern.
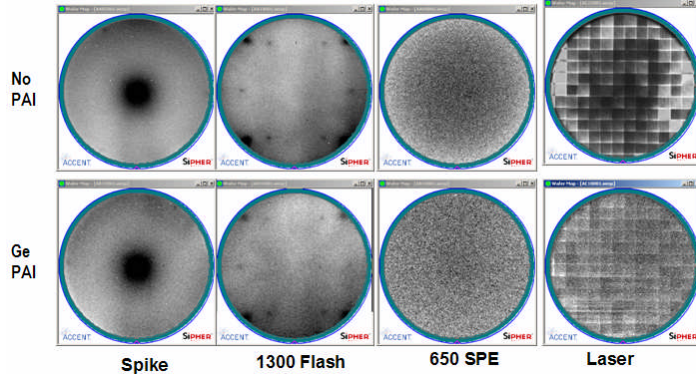


**Figure 8.** PL full wafer map imaging of annealing signatures.

Junction quality/damage recovery was characterized by JPV $R_sL$ leakage measurement. The results are shown in Table 2 (A/cm$^2$) and all the spike and Flash annealed samples with or without Ge-PAI had junction leakage <1E-7A/cm$^2$ (measurement sensitivity limit). The Ge-PAI wafers with laser annealing remained amorphous and the $R_sL$ measured leakage was in the E-2 to E-3A/cm$^2$ range. While without PAI $B_{18}H_{22}$, $B_{10}H_{14}$ and B were in the 1–3E-7A/cm$^2$ range and BF$_2$ was 3E-6A/cm$^2$ due to EOR damage. Results for the SPE anneal showed that an excellent junction leakage current of 2E-7A/cm$^2$ measured for the $B_{10}H_{14}$ and $B_{18}H_{22}$ wafers suggests high quality junctions. The Ge-PAI wafers were in the E-5A/cm$^2$ level. The

B and BF$_2$ wafers were in the E-5 and E-6A/cm$^2$ range due to residual damage and EOR damage after SPE annealing.

**Table 2.** JPV junction leakage measurements (A/cm$^2$)

| Dopant | Spike/1080 | Spike/1000 | Flash | Laser | SPE |
|---|---|---|---|---|---|
| B | 1E-7 | 1E-7 | 1E-7 | 3E-7 | 1E-5 |
| +PAI | 1E-7 | 1E-7 | 1E-7 | 2E-2 | 6E-6 |
| BF2 | 1E-7 | 1E-7 | 1E-7 | 3E-6 | 1E-6 |
| +PAI | 1E-7 | 1E-7 | 1E-7 | 1.5E-3 | 1E-5 |
| B10-serial | 1E-7 | 1E-7 | 1E-7 | 2E-7 | 2E-7 |
| +PAI | 1E-7 | 1E-7 | 1E-7 | 1.8E-3 | 3E-5 |
| B10 | 1E-7 | 1E-7 | 1E-7 | 1E-7 | 2E-7 |
| +PAI | 1E-7 | 1E-7 | 1E-7 | 2.3E-2 | 3E-5 |
| B18 | 1E-7 | 1E-7 | 1E-7 | 1E-7 | 2E-7 |
| +PAI | 1E-7 | 1E-7 | 1E-7 | 2.3E-2 | 2E-5 |

For shallow junctions <25nm deep, an accurate 4PP sheet resistance ($R_s$) measurement for dopant activation is very difficult to obtain due to probe penetration of any or all of the probes. Therefore, we compared several new alternative methods to measure $R_s$ (ohms/square). Non-penetrating contact EM-4PP and Hg-4PP $R_s$ results, as well as JPV $R_s$ results are compared to standard 4PP with blunted probe tips and are shown in Table 3. For most of the conditions, good agreement between all the various $R_s$ metrology techniques were verified, however, for some of the conditions, a wide range of $R_s$ values were observed, especially for the B laser and SPE diffusion-less activation anneals even though SIMS analysis detected deep junctions of >24nm. The true electrical junction depth could be much shallower than the SIMS determined junction depth which is based on the B chemical (elemental) depth profile.

**Table 3.** Comparison of various Rs (ohms/sq.) metrology results (Hg/std/EM/JPV).

| Dopant | Spike/1080 | Flash | Laser | SPE |
|---|---|---|---|---|
| B | 342/340/313/315 | 527/525/466/475 | 2200/2224/1209/1100 | 20403/19410/62K/7500 |
| +PAI | 349/340/342/315 | 538/512/473/470 | no p/n | 1227/1135/1235/1080 |
| BF2 | 465/453/466/430 | 661/641/682/610 | 998/806/1378/996 | 4818/4856/4335/3600 |
| +PAI | 534/526/719/488 | 674/675/685/637 | no p/n | 2183/1746/2954/1872 |
| B10-serial | 590/579/535/536 | 905/895/831/791 | 844/988/857/706 | 2680/2676/2456/2175 |
| +PAI | 656/650/614/600 | 860/842/842/759 | no p/n | 1678/1025/1799/1488 |
| B10 | 566/553/538/516 | 809/781/765/732 | 877/832/1494/511 | 2940/2961/3521/2377 |
| +PAI | 617/601/589/560 | 780/791/955/703 | no p/n | 3368/--/1531/1590 |
| B18 | 405/393/378/368 | 539/526/503/484 | 583/580/561/728 | 1781/1785/1682/1493 |
| +PAI | 464/452/640/423 | 613/595/725/555 | no p/n | 1384/1099/1400/1239 |

From the $R_s$ vs. $X_j$ plot, the dopant activation level was determined [5]; however, since there is always uncertainty in the true electrical junction depth, as well as the measured $R_s$ value by each of these techniques, there is uncertainty in the true

activated level. The determined dopant activation level also known as the boron solid solubility limit ($B_{ss}$) is listed in Table 4 [a) Nsurf and b) Bss derived from Rs-vs.-Xj]

**Table 4.** Carrier density /cm$^3$ determined by Nsurf or Bss (Rs/Xj)

| Dopant | | Spike/1080 | Spike/1000 | Flash | Laser | SPE |
|--------|------|-----------|-----------|-------|-------|-----|
| B | Nsurf | 1.9E19 | 1.8E19 | 4.4E19 | 1.2E20 | 9E18 |
| | Bss | 7-8E19 | 5E19 | 1E20 | 2-4E19 | <8E18 |
| +PAI | Nsurf | 5.5E19 | 7.2E19 | 9.5E19 | no p/n | 4.6E19 |
| | Bss | 7-8E19 | 5E19 | 9E19 | no p/n | 6E19 |
| BF2 | Nsurf | 3.9E19 | 3.7E19 | 6.3E19 | 1.3E20 | 1.8E19 |
| | Bss | 8E19 | 3-4E19 | 8E19 | 4-7E19 | 1.5E19 |
| +PAI | Nsurf | 4.4E19 | 4.6E19 | 8.6E19 | no p/n | 1.4E19 |
| | Bss | 8E19 | 3-4E19 | 1E20 | no p/n | 3-4E19 |
| B10-serial | Nsurf | 4.8E19 | 6.3E19 | 9.2E19 | 1.6E20 | 7.4E19 |
| | Bss | 7E19 | 4E19 | 0.9-1E20 | 7-9E19 | 3-4E19 |
| +PAI | Nsurf | 4.2E19 | 5.2E19 | 8.9E19 | no p/n | 4.8E19 |
| | Bss | 7E19 | 3-4E19 | 8E19 | no p/n | 6E19 |
| B18 | Nsurf | 4.2E19 | 4.7E19 | 9.7E19 | 1.4E20 | 6.3E19 |
| | Bss | 8E19 | 4-5E19 | 1.3E20 | 0.9-1.3E20 | 4E19 |
| +PAI | Nsurf | 5.2E19 | 5.3E19 | 1.2E20 | no p/n | 3.9E19 |
| | Bss | 7-8E19 | 3-4E19 | 0.9-1.2E20 | no p/n | 6E19 |

The wide spread in $B_{ss}$ values for a specific annealing technique is due to the wide range in $R_s$ values determined by the various metrology techniques listed in Table 3. PAI+B with a 1000$^o$C spike anneal $R_s$ determined $B_{ss}$ varied from 0.5-1E20/cm$^3$ and PAI+BF$_2$ with SPE anneal $B_{ss}$ varied from 2.5–5E19/cm$^3$. For this reason, a new technique to directly measure the near surface electrically active dopant density (Nsurf) within the top 3nm of the surface was developed using an EM-probe CV based technique. Using this technique, we could directly measure the surface activated dopant density, and therefore compare each implant species and annealing conditions without having to know the electrical junction depth.

Table 4 also shows Nsurf results. The highest Nsurf dopant activation levels were seen with laser annealing (1.6E20/cm$^3$) followed by flash (1.2E20/cm$^3$), and then spike annealing (7.5E19/cm$^3$), and SPE (7.4E19/cm$^3$) as shown in Fig. 9. For each annealing technique, the highest dopant activation was always detected for the molecular dopant species without Ge-PAI, while the opposite conclusion would be made using $B_{ss}$ determined from the $R_s$ vs. $X_j$ data in Table 4. Except for the SPE annealing case, the $B_{ss}$ values were similar, with or without Ge-PAI for the spike and Flash anneals. For SPE anneals, the Ge-PAI wafers always had higher $B_{ss}$ activated levels. For most of the cases good agreement was observed between Nsurf and Rs/Xj determined Bss as shown in Table 4. However, for some cases like the B spike annealed at both 1080$^o$C and 1000$^o$C the difference between Nsurf and Bss was as much as 4x (1.9E19/cm$^3$ versus 8E19/cm$^3$). The SIMS profile in Fig. 1a showed B diffusion at approximately 1.5E20/cm$^3$ with a surface pile-up of 2E21/cm$^3$ of electrically inactive B. Spreading resistance depth profile (SRP) was conducted on this sample by beveling. A drop in the electrical active dopant level towards the surface is clearly observed by SRP in agreement with the lower Nsurf measurement shown in Table 4.
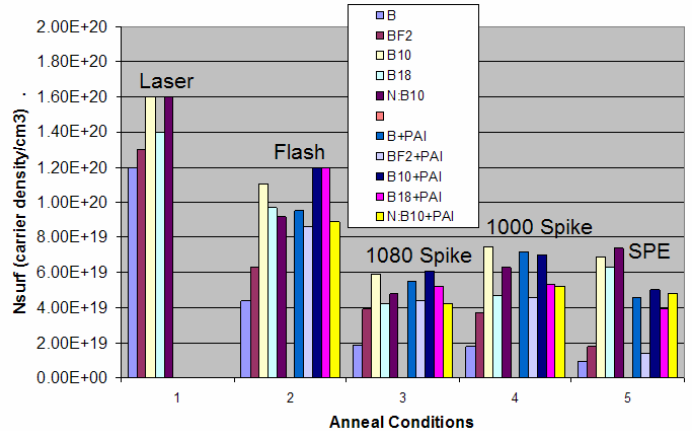


**Figure 9.** Nsurf for various anneals.

## CONCLUSION

High quality and high dopant activation p+ junctions ~15-20nm deep can be achieved using $B_{10}H_{14}$ or $B_{18}H_{22}$ with high temperature (>1300$^o$C) flash or laser annealing, as well as low temperature SPE annealing at 650$^o$C. These anneals enable the extension of beam-line implantation to beyond 32nm node with energies at 5–10keV. Residual implant damage when using B, BF$_2$ or Ge-PAI implants make them undesirable with laser and SPE activation due to degradation in junction leakage current. Therefore, molecular dopant species are very attractive for SiON gates using fast (msec) or ultra-fast (200nsec) annealing, or high-$k$ Hf-oxide gates requiring low thermal budget processing (low temperature spike or SPE annealing). New USJ metrology techniques were evaluated and found to be critical in determining the junction quality and dopant electrical activation level.

### REFERENCES

[1]. F. Ootsuka, H. Ozaki, T. Sasaki, K. Yamashita, H. Takada, N. Izumi, Y. Nakagawa, M. Hayashi, K. Kiyono, M. Yasuhira and T. Arikado, *IEDM 2003*, section 27.7, p. 647.
[2]. R. Surdeanu, R. Lindsay, S. Severi, A. Satta, B. Pawlak, A. Lauwers, C. Dachs, K. Henson, S. McCoy, J. Gelpey and X. Pages, *SSDM 2004*, section B-3-1, p. 180.
[3]. J. Borland, M. Tanjo, N. Nagai, T. Aoyama and D. Jacobson, *Semiconductor International*, Jan. 2005, p. 52.
[4]. T. Aoyama, M. Fukuda, Y. Nara, S. Umisedo, N. Hamamoto, M. Tanjo and T. Nagayama, *IWJT 2005*, June 2005, section S2-2, p. 27.
[5]. J. Borland, T. Matsuda and K. Sakamoto, *Solid State Technology*, June 2002, p. 83.